Aicha Zouaneb,
Elfahem Sakher,
Rachid Tigrine,
Abdallah Bendoura,
Aissa Benselhoub

CONSIDERATION OF ELECTRONIC MEAN HEAT TRANSPORT VIA A LOW DIMENSION SYSTEM

The object of research is the complex realm of energy localization and coherent ballistic electronic transport within low-dimensional silicon quantum wires, specifically those doped with germanium atoms. Unlike their three-dimensional counterparts, low-dimensional systems exhibit unique electronic transport behaviors, necessitating novel analytical approaches for a comprehensive understanding. The core of this investigation leverages the Phase Field Matching Theory (PMFT) and the tight-binding (TB) approximation, sophisticated methodologies that enable a deep dive into the quantum mechanical nuances of these systems. Through this lens, we examine the intricate dynamics of dispersion relationships, phase factors, group velocities, and notably, the impact of defects introduced by the germanium doping.

This research meticulously analyzes how these defects affect electronic and thermal conductivities, along with densities of states, offering new insights into the role of Fano resonances in the fluctuation of transmission and reflection spectra. These resonances, we find, are crucially dependent on the nature of the defects, their configuration, and the electronic parameters in their vicinity, underscoring the nuanced interplay between material composition and electronic properties in low-dimensional systems.

The implications of our findings extend far beyond the theoretical. They pave the way for significant advancements in nanotechnology and the design of electronic devices, highlighting the potential for creating more efficient, high-performance components. Furthermore, this work proposes a framework for developing non-destructive testing methodologies that could revolutionize material science by enabling the precise analysis of defects in low-dimensional systems without causing damage. This is particularly critical for the ongoing development of materials with optimized properties for various applications, from electronics to energy storage.

In essence, this research not only enriches our understanding of the physics governing low-dimensional systems but also offers practical insights into leveraging these properties for technological innovation. By bridging the gap between theoretical physics and material science, our study sets the stage for the next generation of electronic components and non-destructive evaluation techniques, marking a significant step forward in the application of quantum mechanics to real-world challenges.

Keywords: *Phase Field Matching Theory (PMFT), tight-binding (TB), Landauer Büttiker formalism, Green's functions.*

1. Introduction

There are several advantages regarding the electronic study of silicon which makes it motivating such as (abundance on the earth, low price charge, non-toxicity, easy and smooth doping, etc.). The cells produced industrially reach a conversion efficiency of 15 per cent on average (modules at 11-per cent) [1].

Thus, according to Moore's Law, the continuous miniaturization of transistors empirically characterizes the exponential trend over fifty years. It has globally made an unprecedented development conceivable by experimental exploration and technological mastery of the microscopic field of matter. It is looking at the unquestionable silicon as the primary key material of this industrial boom, whose electronic properties have made it the Bedrock of insulated-gate field-effect transistors. However, this systematic reduction in the standard size of the electronic components cannot continue indefinitely, the single-atom transistor [2] being the ultimate physical limits. It expects a paradigm shift in the coming decades, on which many research teams composed of physicists, concentrated engineers and chemists. Concerning this Perspective of considerable studies and abundant research of new and recent high-performance materials, numerical simulation occupies a vital place, furthermore, from the early 1970s atomistic methods whose improvement exploded. Thanks, in component to this same Moore's law which are specially adapted. Their reliable predictive power linked to the degree of low

approximation of the Fundamental underlined theories and evident ability describing the accurate nanometer-scale of the materials, which gives it the cardinal approaches towards the experimental complement. Since experiences and simulations go together simultaneously; too often separated in research laboratories, both approaches can help each other, and whose symbiosis catalyzes scientific and industrial development and improvement. In micro-electronics, several problems are associated with transporting phenomena, the capping of the frequent clock processors [3, 4]. Notably, the dynamic nature of transport phenomena makes them difficult towards the model. However, over the past and previous thirty years, has in many ways been developed. Comprehensive, universal and critical properties, such as thermal and electronic conductivities introduction allow getting more or less accurately [5, 6]. Recently, nano-science, nano-technology and nano-materials are booming and make up a transversal domain between physics, chemistry and many other scientific and industrial fields and aspects. In respect to this, the electronic quantum transport properties in nanostructures are essential for the development of nano-electronic devices [7, 8] as an element connecting between these components [9]. Whether chemical or structural, however, impurities have familiar places in nano-materials where they have locations that are not predictable. Their appearance effects and changes different physical quantities [10, 11]. For example, there can be a notable impact on ballistic coherent transport properties in a nano-junction [10], chemical defects or substitution disorder. Furthermore, there will be an appearance the localized and scattered states in the defect region as well as in bulk far from the disturbed area. The transportation of these nanostructures can even be controlled by doping chemical impurities [12]. Hence, the nano-electronic device properties and its functionality can be significantly affected or also constructed in such an ordered and disordered configuration. In correspondence compared with the properties of solids, there is a significant change between the physical properties of nano-materials. The understandings towards the nano-materials physical properties were due to the presence of a defect, and the nanoscale prompted physicists and chemists strictly depending on their structures.

In describing them, it is essential to utilize and exploit several current adapted methods, such as the Phase Field Matching Theory (PFMT) [13–15] which is an excellent tool for the study of electronic quantum transport in nano-materials with breaking symmetries. It is useful when determining the scattering probabilities for the transmission and reflection process of electrons, as well as quantum particles according with the Landauer-Büttiker formalism [16–18]. This approach illustrates the electronic properties in the tight-binding approximation context (TBA), which is used widely for electronic and automatic calculations for transport [12, 19–21].

In aforementioned of this work, through a nano-wire consisting of an atomic chain of silicon doped with a single atom of germanium, the problem of coherent ballistic electronic transport was examined. The tight-binding theory is an efficient and effective method towards the study of the perfect system far from defect. Moreover; it is possible to write the secular equations with this approximation for our system where the atomic orbital s and p_x have chosen in the present case. In particular, let's use Slater-Koster Hamiltonian parameters [22] calculated by Harrison's tight-binding theory (HTB) [23]. Due to its transparency and natural forms as a primary and parameterization method for numerical calculations, the HTB method is chosen. Harrison has simplified the linear combination atomic orbitals approach (LCAO) by building universal parameters which can perform the calculations [24]. Moreover, the PFMT with Landauer-Büttiker formalism deals the scattering problem by studying the transmission and reflection probabilities of the incident wave [16, 25]. The PFMT is said to be a powerful mathematical tool that links and connect the electronical conductance to the scattering matrix. Thus, the PFMT method has mainly been adopted by many scientists to study the disorder systems [26, 27]. Lately; at the surface in metallic structures, it was used to determine the localized electronic states [15].

Given the critical advancements in silicon-based technologies and the pressing challenges in miniaturizing electronic components to their physical limits, *this research aims* to address the nuanced mechanisms of electronic transport within doped silicon quantum wires. Recognizing the pivotal role of silicon in the semiconductor industry, driven by its abundance, cost-effectiveness, and superior electronic properties, and the advent of novel phenomena at the nanoscale, our study seeks to transcend traditional analytical paradigms. The Phase Field Matching Theory (PFMT) and tight-binding (TB) approximation are leveraged to unravel the complex interplay of energy localization, ballistic transport, and the implications of germanium doping. This research endeavors to enhance our theoretical understanding of quantum transport mechanisms in low-dimensional systems and to pioneer new pathways for developing next-generation nano-electronic devices. By probing the intricacies of defect-induced variations in electronic and thermal conductivities, our work is positioned to significantly contribute to the advancement of nanotechnology, offering a comprehensive framework for exploring and exploiting the unique properties of nano-materials for innovative electronic applications.

2. Materials and Methods

2.1. Description of study model. The studied system consists of two semi-infinite mono-atomic linear chains of silicon (blue color), where the mesh parameter is the same everywhere. These chains are connected by a single germanium atom (red color) considered as a defect. In this model, each atom is described by tow s and p_x-like atomic orbital. The overlap integrals which describe the interactions between the nearest atoms is noted H_{ij}; such that i, j denote the type of atomic orbital. ε_s and ε_p are the energies of the site «s» and «p_x», respectively and C_α is the wave function coefficient of the site «α». The system is presented in Fig. 1, with the associated physical quantities.
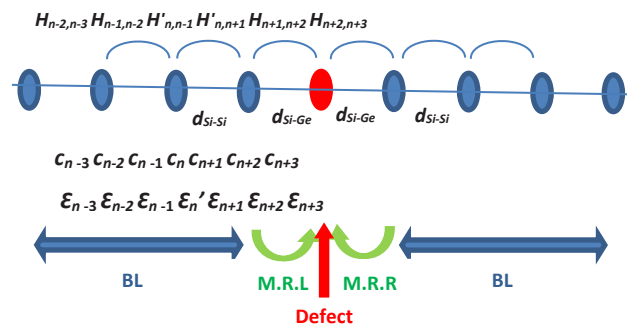
Fig. 1. Schematic representation of a one-dimensional chain of atoms disordered by two bulk leads (BL), two matching regions left and right (MRR and MRL) and one atom defect (red color)

Let's note that each atom has two s and p-like atomic orbital (Fig. 1).

2.2. Methods. It is imperative to understand the electronic transport properties of nano-wire. Otherwise, electronic transport or electronic conductance in solids is bound by the movement of electron in which their behavior may change toward nanostructures. Furthermore, the electrons that contribute to nano junction transport exhibit characteristic wavelengths that are compared towards these components size, leading to coherent quantum effects. The nano-electronic device's properties and their functionality can then be significantly affected or even built on these nano-junctions quantum effects. Still, it cannot be expressed in the context of the conventional regime. Hence, the efficient and accurate determination and perception of transmission and reflection scattering probabilities for electrons, as well as quantum particles, is done from an algebraic phase matching field theory (PFMT).

To study scattering nano-system, let's start by specifying the electronic states for the modeling band structures making use of a tight-binding approximation (also known as TBA), likewise called the combination of linear atomic orbitals (LCAO). From the historical and classical point of view, the contribution to the development of the TBA theory was first given by author of [28]. It is possible to use the tight-binding approximation, the electron transport in a one-dimensional atomic chain that can be expressed in quantum mechanics to a single secular particle by the Schrödinger equation:

$$H\left|\psi_k(\vec{r})\right\rangle = E\left|\psi_k(\vec{r})\right\rangle, \tag{1}$$

where ψ_k – the system's wave function for state k; E – the energy of state k; H – Hamiltonian.

Let's use a base of atomic orbitals that overlap or «hybridize» as:

$$\left|\psi\right\rangle = \sum_{i,n} C_{i,n} \frac{1}{\sqrt{N}} \sum e^{i\vec{k}\cdot\vec{R}}\left|\varphi^n\right\rangle, \tag{2}$$

where $C_{i,n}$ denotes the orbital coefficients, where i is the number of atoms in unit cell and n is the number of orbitals ($n = s, p_x$). Since atomic orbital functions are considered orthogonal:

$$\left\langle\varphi_n^i\middle|\varphi_{n'}^i\right\rangle = \delta_{n,n'}, \tag{3}$$

where

$$\delta_{n,n'} = \begin{cases} 1 & \text{if} \quad n = n', \\ 0 & \text{if} \quad n \neq n'. \end{cases} \tag{4}$$

In the (TB) approximation, it is possible to consider that the nearest-neighbors C_n, C_{n-1}, $C_{n+1} \neq 0$; and the others are void. Equation (1) becomes:

$$H_{ij}c_{n-1} + (\varepsilon_i + V - E)c_n + H_{ij}c_{n+1} = 0, \tag{5}$$

where ε_i – the energy of the orbit i, H_{ij} – the matrix that contains the overlap elements between the atom n and n'.

By introducing Bloch's theory for the electronic structure in the system's bulk that is presented in Fig. 1: $c_{n\pm 1} = e^{\pm i\varphi_\alpha}c_n$ or $e^{\pm i\varphi_\alpha}$ is the phase translation factor along a direction «α»,

it requires a total and comprehensive calculation of the bulk dispersion. Otherwise, equation (5) provides the different eigenvalues but it is necessary to extract the propagation mode, which obeys the condition given by $|Z| = 1$. However, the computation of evanescent modes allows to search for the eigenmodes that capture the condition $|Z| < 1$. On the other hand, the system given by equation (5) generates a rectangular Hamiltonian matrix for the defect area. In this situation, the Hamiltonian matrix comprises an unbalanced number of unknown variables alongside with the number of secular equations. Hence, it is not possible for a direct solution. An adequate method, such as the phase field matching theory (PFMT), is needed. It is an analytical approach that can determine the physical quantities describing disordered systems. It has been introduced as a powerful method to study the equilibrium of low-dimensional systems that integrates the nano-structures and the static structure of a 3D semi-infinite crystal lattice. In early 1967, this method was used for the first time for a study at the equilibrium of a semi-infinite 3D crystal lattice [29]. It was initially developed for the scattering of phonons and magnons in excitation through nano-junction, consequently used for the study of vibrational properties [30]. In 2012, it implemented to study electronic transport [14, 31]. With the matching theory, it is possible to describe the electronic properties of any system, based on the phase matching of the electronic states of the electrodes with those of the nano-junctions. Moreover, this method makes it possible to make use of unit cells of different sizes and shapes to consider systems. It is similar to the different types of excitations by replacing the dynamic equation of phonons or magnons by the Schrödinger equation. It shows that the system has been divided into three central regions according to the application of the matching method, namely the nano-junction region or the defect zone and two other leads on the right and left of the nano-junction which are the matching zones (MRL and MRR) and the bulk (BL).

For the eigenmode i, from left to right, the propagating electron wave incident can be reflected or transmitted. Moreover, for an outside atom bordering the defect source and due to the displacement in both sides, using the matching approach as a function of the phase factor «Z» as well as the bulk eigenvectors «U_l and U_r» the wave function coefficients will be expressed. The linear coefficients C_n^l of the atomic orbitals forming the system's wave function can be shown for the left matching as the sum of the incident wave and a superposition of the eigenvectors of the reflected perfect wave:

$$c_n^l = \sum_{v=1}^{v} c_v\left[Z^{-n}U_l\right] + Z^n c_v, \tag{6}$$

where v – the number of the bulk eigenmode U_l denotes the eigenvector of the bulk matrix and Z is the phase factor.

For a site within the electron wave to the right of the defect, the atomic coefficients C_n^r can be expressed by an appropriate superposition of the eigenvectors of the perfect transmitted wave:

$$c_n^r = \sum_{v=1}^{v} c_v\left[Z^n U_r\right], \tag{7}$$

where U_r denotes the eigenvector of the bulk matrix.

From equations (5), (6) and (7) used next to transform the rectangular Hamiltonian matrix for the defect area into an inhomogeneous square matrix for the scattering problem (6×6):

$$G = \frac{2e^2}{h} \sum_i T_i. \tag{8}$$

This matrix solution yields the transmissions and reflections probabilities where the total transmission makes it possible to calculate the global electronic conductance across the defect, which is given by the basic and essential Landauer-Büttiker relation.

3. Results and Discussions

In this section, numerical calculations are presented for quantic wire of silicon doped by an impurity of germanium. The different physical properties determined by our calculation model are presented, where the atoms are characterized by the electronic states $3s$ and $3p$ for silicon and by $4s$ and $4p$ for germanium. Their orbitals hybridization is s and p_x for both types of atoms. The TB parameters are rescaled used in this work according to Harrison data, which it presents in Table 1.

Table 1

Hopping parameters used in this work from [23]

Atom type	α	Ge	Si
On-site matrix elements (eV)	ε_s	−15.16	−14.79
	ε_p	−7.33	−7.59
Types of interaction between nearest neighbors	χ	Si-Ge	Si–Si
Distance interatomic between nearest-neighbors	$d_\chi(A°)$	2.33	2.2
Hopping parameters (eV)	$V_{ss\sigma}$	−1.85	−2.08
	$V_{sp\sigma}$	1.99	2.24
	$V_{pp\sigma}$	3.12	3.50

In Table 1, α denotes the atom type; Ge or Si, the on-site matrix elements and the hopping parameters are calculated as follows:

$$\varepsilon_{n,n'}^{l,l'} = \left\langle \varphi_n^l(r - R_n) \middle| \varphi_{n'}^{l'}(r - R_{n'}) \right\rangle,$$
$$\left\langle \varphi_n^l(r - R_n) \middle| H \middle| \varphi_{n'}^{l'}(r - R_{n'}) \right\rangle = V_{ll',nn'}\delta(R_{n'} - R_n). \tag{9}$$

The index χ represents the types of interaction between nearest neighbors, Ge–Ge, Si–Si or Si–Ge and the Hopping elements are expressed by Harrison's tight-binding theory as:

$$V_{l,l',m}^{n,n',\chi} = \eta_{l,l',m} \frac{\hbar^2}{m_e d_\chi^2}, \tag{10}$$

where $\eta_{l,l',m}$ – the Harrison coefficients, m represents the band type σ or ϖ between l and l' which represent two different atomic sites, m_e refers to the electron vacuum mass, $d\chi$ – the distance interatomic between nearest-neighbors or it is possible to use directly $\hbar^2/m_e = 7.62$ eV·Å^2.

Let's note that the Harrison coefficients $\eta_{l,l',m}$ used in this paper are; $\eta_{sss} = -1.32$, $\eta_{sps} = 1.42$ and $\eta_{pps} = 2.22$ for all hybridization type.

3.1. Electronic properties in the bulk

3.1.1. The dispersion relationship. To determine the system's band structure, it is necessary to write the secular equation that has a size equal to the total number of orbits per unit cell. The application of the equation (5) obtained by TB approximation on an atom in the bulk presented in Fig. 1, where:

$$|\psi\rangle = c_n \sum_l \sum_R e^{i\vec{k}.\vec{R}} |\varphi_l^n\rangle + c_{n+1} \sum_l \sum_R e^{i\vec{k}.\vec{R}} |\varphi_l^{n+1}\rangle +$$
$$+ c_{n-1} \sum_l \sum_R e^{i\vec{k}.\vec{R}} |\varphi_l^{n-1}\rangle. \tag{11}$$

Leads to the two following equations:
– for $|\varphi^n\rangle = |\varphi^s\rangle$:

$$(\varepsilon_s + V - E) + c_{n-1}\langle\varphi_n^s|H|\varphi_{n-1}^s\rangle + c_{n-1}\langle\varphi_n^s|H|\varphi_{n-1}^{p_x}\rangle +$$
$$+ c_{n+1}\langle\varphi_n^s|H|\varphi_{n+1}^s\rangle + c_{n+1}\langle\varphi_n^s|H|\varphi_{n+1}^{p_x}\rangle = 0; \tag{12}$$

– for $|\varphi^n\rangle = |\varphi^{p_x}\rangle$:

$$(\varepsilon_p + V - E) + c_{n-1}\langle\varphi_n^{p_x}|H|\varphi_{n-1}^s\rangle + c_{n-1}\langle\varphi_n^{p_x}|H|\varphi_{n-1}^{p_x}\rangle +$$
$$+ c_{n+1}\langle\varphi_n^{p_x}|H|\varphi_{n+1}^s\rangle + c_{n+1}\langle\varphi_n^{p_x}|H|\varphi_{n+1}^{p_x}\rangle = 0. \tag{13}$$

Introducing Bloch's theory in the x direction yields a matrix of order (2×2) as following:

$$E = \begin{pmatrix} A+\omega & B \\ -B & C+\omega \end{pmatrix}, \tag{14}$$

where

$$A = (2\cos\varphi_x), \tag{15}$$

$$B = (2i\sin\varphi_x)\frac{V_{sp\sigma}}{V_{ss\sigma}}, \tag{16}$$

$$C = (2\cos\varphi_x)\frac{V_{pp\sigma}}{V_{ss\sigma}} + (\varepsilon_p - \varepsilon_s)/V_{ss\sigma}, \tag{17}$$

$$\omega = \frac{(\varepsilon_s + V - E)}{V_{ss\sigma}}. \tag{18}$$

The dispersion curve $E = E(\varphi_x)$ for our mono-atomic chain, in the first Brillouin zone is given in Fig. 2 with $\varphi_x \in [-\pi, \pi]$.
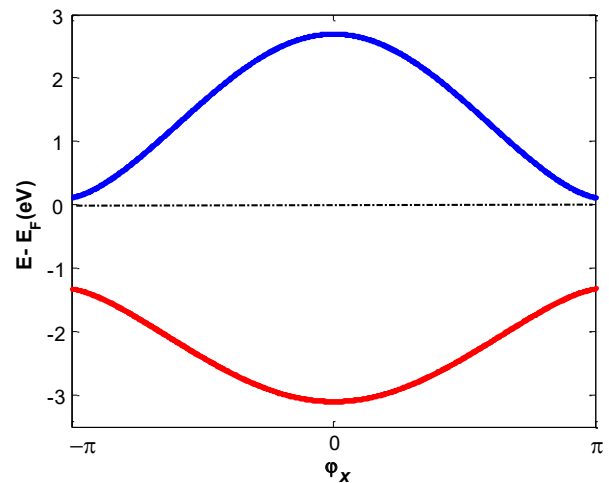
Fig. 2. Representation of dispersion curve for a mono-atomic silicon chain with a single germanium defect described as s and p_x-type orbital. The Fermi level is set at the zero energy reference position

It is clearly seen that there is symmetry regarding ($\varphi_x = 0$) for each curve. These curves are continuous and represent two energy bands; the red and blue colors correspond respectively to the π and σ bands, arise from the *spx* orbital hybrids. In this work, the computed electronic band structures in the bulk system using TBA yielded a direct gap corresponding to the valence band maximum of ($E_v = -1.32$ eV) and the conduction band minimum of ($E_c = 0.13$ eV). These occurred at the $\varphi_x = -\pi$ and $\varphi_x = \pi$ points, respectively.

3.1.2. Eigenvalues and eigenvectors. To determine the matching matrix, it is necessary to explain the displacement of the matching region as a function of the specific eigenvectors and eigenvalues, induced by the study of the electronic properties at the bulk by the TB method. This approximation applied for one site at the bulk and its other N neighborhoods atoms fold up to the chosen site via the phase factor Z where; $Z = e^{i\varphi_x}$, $Z^{-1} = e^{-i\varphi_x}$ and the hopping parameters mentioned in equation (9). The equations (12) and (13) become:

– for $|\varphi_n\rangle = |s\rangle$:

$$(\varepsilon_s + V - E)|s\rangle + V_{ss\sigma}Z^{-1}|s\rangle - V_{sp\sigma}Z^{-1}|p_x\rangle =$$
$$= -V_{ss\sigma}Z|s\rangle - V_{sp\sigma}Z|p_x\rangle; \qquad (19)$$

– for $|\varphi_n\rangle = |p_x\rangle$:

$$(\varepsilon_p + V - E)|p_x\rangle - V_{sp\sigma}^*Z^{-1}|s\rangle + V_{pp\sigma}Z^{-1}|p_x\rangle =$$
$$= -V_{sp\sigma}^*Z|s\rangle - V_{pp\sigma}Z|p_x\rangle. \qquad (20)$$

With an increase of the base as:

$$|s\rangle = \varphi_1, \quad |p_x\rangle = \varphi_2, \quad -\frac{|s\rangle}{Z} = \varphi_3, \quad -\frac{|p_x\rangle}{Z} = \varphi_4.$$

Equations (19) and (20) can be expressed in the following matrix form:

$$\begin{pmatrix} \omega & 0 & -1 & A_{14} \\ 0 & \omega+\delta & A_{23} & A_{24} \\ -1 & 0 & 0 & 0 \\ 0 & -1 & 0 & 0 \end{pmatrix} \times \begin{pmatrix} \varphi_1 \\ \varphi_2 \\ \varphi_3 \\ \varphi_4 \end{pmatrix} =$$
$$= Z \begin{pmatrix} -1 & -A_{14} & 0 & 0 \\ -A_{23} & A_{24} & 0 & 0 \\ 0 & 0 & 1 & 0 \\ 0 & 0 & 0 & 1 \end{pmatrix} \times \begin{pmatrix} \varphi_1 \\ \varphi_2 \\ \varphi_3 \\ \varphi_4 \end{pmatrix}, \qquad (21)$$

where

$$A_{14} = \frac{V_{sp\sigma}}{V_{ss\sigma}}, A_{23} = \frac{V_{sp\sigma}^*}{V_{ss\sigma}},$$
$$A_{24} = \frac{-V_{pp\sigma}}{V_{ss\sigma}}, \delta = \frac{\varepsilon_p - \varepsilon_s}{V_{ss\sigma}}. \qquad (22)$$

General phase factors are the solutions of the system matrix (21). In Fig. 3, the absolute value of the phase factor is represented as a function of ω for the various bulk modes in Fig. 3. There is an electron wave propagation represented by a line parallel to the x axis, where the propagating modes are in the range of $\omega \in [0, 2.15]$ for

mode 1 and $\omega \in [0, 3.83]$ for mode 2. On these ranges, the electronic waves cross the system without attenuation (by the way). In addition, there is an evanescent mode which has an exponential form, represented by the decreasing curve until it is vanished. The evanescent modes are from $\omega = 2.15$ and $\omega = 3.83$, where the system acts like a mirror and don't let the waves pass through it.
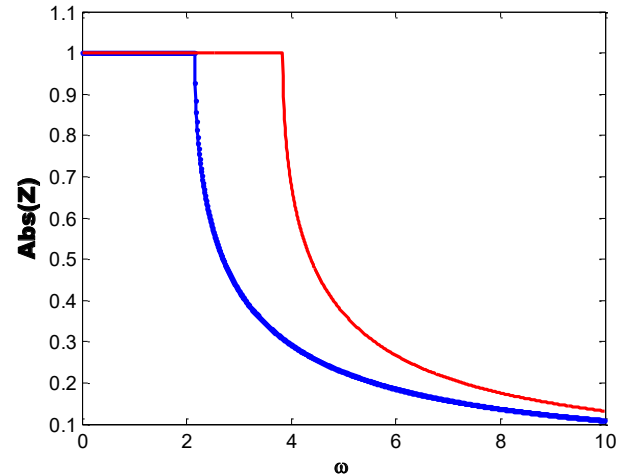
Fig. 3. The variation of the absolute values phase factor versus ω; (blue color) for state 1 and (red color) figured state 2

3.1.3. The group velocity. The speed of energy displacement for our model system is defined by υ_g:

$$\upsilon_g = \frac{\partial B}{\partial \varphi_x}. \qquad (23)$$

Such as B: the bulk matrix element:
– for $|\varphi_n\rangle = |s\rangle$:

$$\upsilon_g = i(Z - Z^{-1})V_{ss\sigma}|s\rangle + i(Z + Z^{-1})V_{sp\sigma}|p_x\rangle; \qquad (24)$$

– for $|\varphi_n\rangle = |p_x\rangle$:

$$\upsilon_g = i(Z + Z^{-1})V_{sp\sigma}^*|s\rangle + i(Z - Z^{-1})V_{pp\sigma}|p_x\rangle. \qquad (25)$$

The evolution of the group velocity as a function of ω is presented in Fig. 4. The group velocity which ensures the transmission of energy in the system in the frequencies band similar to the propagating modes; where the phase factor modulus $|Z| = 1$, $\omega \in [0, 2.15]$ for state 1 and $\omega \in [0, 3.83]$ for state 2 for υ_{g1} and υ_{g2} respectively. It is zero ($\upsilon_g = 0$) for other values (evanescent mode) where the phase factor modulus $|Z| < 1$. This confirms the existence of propagating and evanescent modes in the bulk region in a perturbed mono-atomic chain. Though the evanescent modes do not transport energy like the propagating one, but they are necessary for a complete description of scattering formalism.

3.2. Electronic scattering. The electronic scattering is studied at the perturbed domain with incident electron waves from the left of the adsorbed atomic chain to the right zone in Fig. 1, which is split into its transmitted and reflected parts.
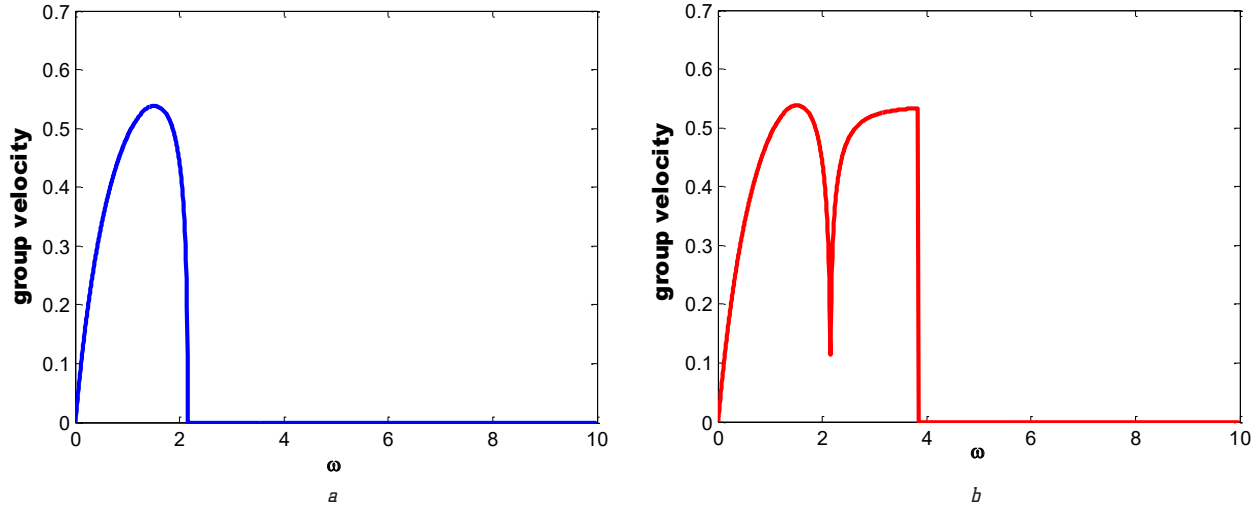
Fig. 4. The variation of the group velocity as a function of ω: a – for υ_{g1}; b – for υ_{g2}

The PFMT is an adapted method to determine the electronic scattering properties via the disturbed zone in our system between the germanium defect and these nearest neighbors (silicon atoms) left and right by writing the secular equations for each atom like the following one:

$$\begin{cases} \langle \varphi_s^n | H | \psi \rangle = \langle \varphi_s^n | I | \psi \rangle, \\ \langle \varphi_{p_x}^n | H | \psi \rangle = \langle \varphi_{p_x}^n | I | \psi \rangle, \end{cases} \qquad (26)$$

where

$$\langle \varphi_s^n | H | \varphi_s^{n+1} \rangle = H_{ss} = V_{ss\sigma},$$

$$\langle \varphi_s^n | H | \varphi_{p_x}^{n+1} \rangle = H_{sp_x} = l V_{sp\sigma},$$

$$\langle \varphi_{p_x}^n | H | \varphi_{p_x}^{n+1} \rangle = H_{p_x p_x} = l^2 V_{pp\sigma} + (1-l) V_{pp\pi}. \qquad (27)$$

While the coefficient l refers to the Cartesian cosine directions: $l = \cos\theta \cdot \cos\varphi$.

The defect study gives rise to a matrix system of 6 rows and 10 columns:

$$D = \begin{pmatrix} h_{11} & 0 & h_{13} & h_{14} & h_{15} & h_{16} & 0 & 0 & 0 & 0 \\ 0 & h_{22} & h_{23} & h_{24} & h_{25} & h_{26} & 0 & 0 & 0 & 0 \\ h_{31} & h_{32} & h_{33} & 0 & 0 & 0 & h_{37} & h_{38} & 0 & 0 \\ h_{41} & h_{42} & 0 & h_{44} & 0 & 0 & h_{47} & h_{48} & 0 & 0 \\ h_{51} & h_{52} & 0 & 0 & h_{55} & 0 & 0 & 0 & h_{59} & h_{510} \\ h_{61} & h_{62} & 0 & 0 & 0 & h_{66} & 0 & 0 & h_{69} & h_{610} \end{pmatrix}, \qquad (28)$$

where

$$h_{11} = (\varepsilon_s' + V - E), \; h_{13} = h_{15} = h_{31} = h_{51} = 2\cos\varphi_x V_{ss\sigma}',$$

$$h_{14} = h_{16} = h_{32} = h_{52} = 2i\sin\varphi_x V_{sp\sigma}', \; h_{22} = (\varepsilon_p' + V - E),$$

$$h_{23} = h_{25} = h_{41} = h_{61} = 2i\sin\varphi_x V_{sp\sigma}'^*,$$

$$h_{24} = h_{26} = h_{42} = h_{62} = 2\cos\varphi_x V_{pp\sigma}',$$

$$h_{33} = h_{55} = (\varepsilon_s + V - E), \; h_{37} = h_{59} = 2\cos\varphi_x V_{ss\sigma},$$

$$h_{38} = h_{510} = 2i\sin\varphi_x V_{sp\sigma}, \; h_{44} = h_{66} = (\varepsilon_p + V - E),$$

$$h_{47} = h_{69} = 2i\sin\varphi_x V_{sp\sigma}^*, \; h_{48} = h_{610} = 2\cos\varphi_x V_{pp\sigma}. \qquad (29)$$

The system of equation (29) has no solution. It is necessary to reduce it to a system with several unknowns and equations.

To analyze the scattering in the presence of defect, it is necessary to know the propagating modes, and also to consider the evanescent solutions of our system. With the Phase Field Matching Theory, it is possible to write the coefficients C_n of the left and right matching regions as a function of Z which was defined before in bulk and the eigenvectors U_r and U_l. A matching matrix (R) of order (10×6) is obtained. Using the defect and matching matrixes, it is also possible to obtain a numerically soluble square matrix (M) with 6 rows and 6 columns:

$$M(6 \times 6) = D(6 \times 10) \times R(10 \times 6). \qquad (30)$$

Due to the fact that the scattering phenomena are related to the incident electronic wave from the left (Si) lead to the right passing through the (Ge) defect, this latter has a footprint on the transmission and reflection coefficients presented by curves (Fig. 5).

The transmission and reflection coefficients curves are of nonlinear form with tow Fano resonances, resulting from the coupling between the localized defect states and the bulk propagating modes. They spread respectively on the interval of $\omega \in [0, 2.15]$ for the first state and $\omega \in [0, 3.83]$ for the second state, and they vanished at the limit of propagating zone according to the beginning of evanescence area. In particular, for state 1 at $\omega_F = 2.034$ and for state 2 at $\omega_F = 1.448$, it assigns a Fano resonance. The results obtained show that the transmission spectrums decrease due to the electric wave moving through the system. Contrariwise, the reflections increase at the beginning of scattering to reach a maximum at the limit of propagating band.

Furthermore, for the incident electron wave for an eigenmode i, it is possible to calculate the reflection and transmission amplitudes $r_{ii'}$ and $t_{ii'}$ which, are normalized with respect to the group velocities υ_{gi} and $\upsilon_{gi'}$ in the form:

$$r_{ii'} = (\upsilon_{gi'} / \upsilon_{gi}) |R_{ii'}|^2, \; t_{ii'} = (\upsilon_{gi'} / \upsilon_{gi}) |T_{ii'}|^2. \qquad (31)$$

In addition, the total electronic transmission and reflection probabilities for an eigenmode are the sum over all the contributions:

$$r_i = \sum_{i'=1} r_{ii'}, \; t_i = \sum_{i'=1} t_{ii'}. \qquad (32)$$
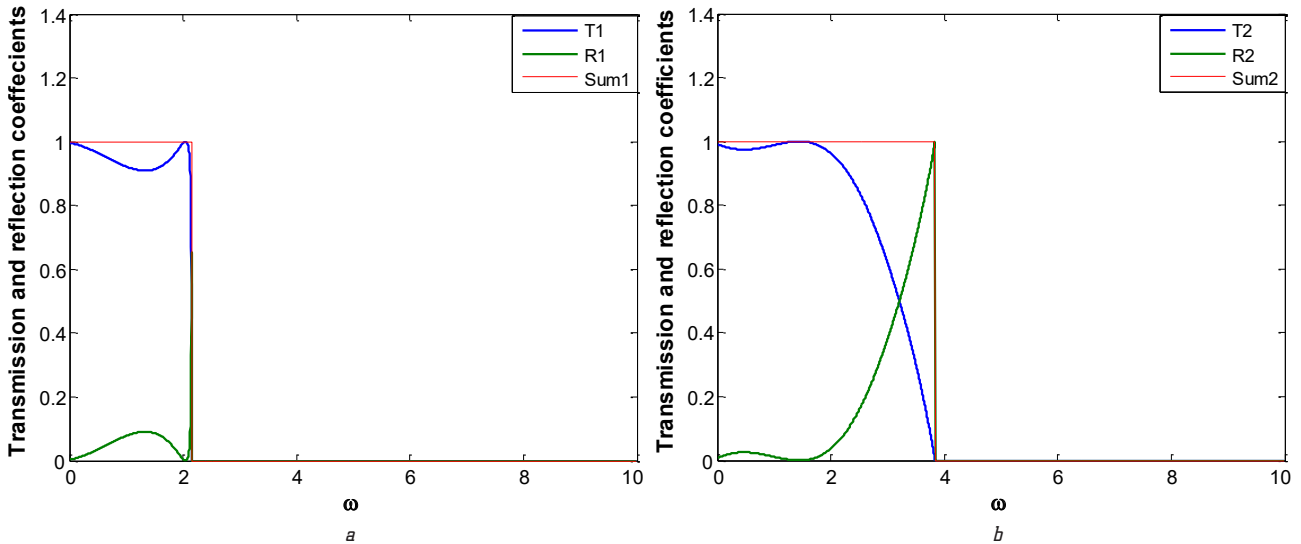
Fig. 5. The evolution of the transmission and reflection coefficients: *a* — for state 1; *b* — for state 2

To compare theory and measurement, the unitarity condition $r_i + t_i = 1$ is used. It checks our numerical calculation.

To describe the overall transmission, it is useful to define the system conductance, which is expressed as the sum of the individual transmission coefficients, carried out over all input and output channels:

$$\sigma(\omega) = \sum_i \sum_{i'} t_{ii'}(\omega). \qquad (33)$$

The resulting electronic conductance of our studied system $\sigma(\omega)$, where the sum is carried out over all propagating modes is shown in Fig. 6.
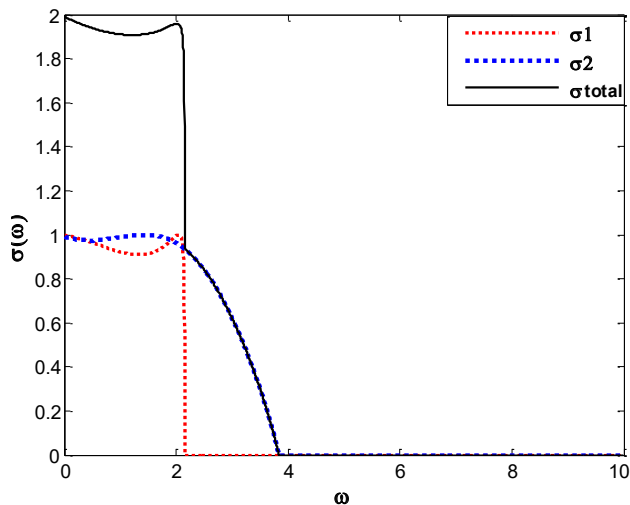
Fig. 6. The electronic conductance curve as a function of ω for a monoatomic Si chain with Ge defect for state 1 (red color), state 2 (blue color) and total (dark color)

In these curves, the conductance spectrum (σ_1 and σ_2) starts with their higher values at $\omega = 0$, fluctuate for excitation energies belonging to the interval [0, 3.83]. In addition, the total conductance which is the sum of the tow contributions σ_1 and σ_2, exceeds unity; it started with 2 in the range of $\omega \in [0, 2.15]$ where the two states overlap. For state 1, the conductance vanished at $\omega = 2.15$ and for state 2, it decreased with increasing ω then becomes zero at the limit of propagating zone for $\omega = 3.83$. This variation

in the electronic conductance is caused by the multiple reflections on the edges of the disturbed area.

3.3. Thermal conductivity. The study of electronic transport at low dimension systems has led to the discovery of many fascinating aspects of quantum resistance. Linking charge transport in the different geometrical configuration confined to a quantum transmission problem, developed by Landauer in a series of papers beginning some twenty years ago [32], was a theoretical idea of unification importance. The idea, in its modern understanding [33], can be expressed in terms of a formula for conductivity between two ideal electrodes. The thermal conductivity depends mainly on the material and the temperature. In general, it goes hand in hand with electronic conductance. From an atomic point of view, it links thermal conductivity to two types of behavior: the motion of charge carriers, electrons or holes and the oscillations of atoms around their equilibrium position. In metals, the free electron movement is predominant, whereas with nonmetals, the vibration of the ions is the most important. It, therefore, links the thermal conductivity, on the one hand, to the electronical conductivity (movement of charge carriers) and to the structure of the material itself (vibrations of atoms or phonons). In our work, let's consider only the thermal conductivity due to the electron of the atoms and to do this, let's start with the calculation of the electronic conductance, which is an essential parameter for the calculation of the thermal conductivity. The waveguide conductance $\sigma(\omega)$, the Fermi-Dirac distribution $n(T, \omega_i(q))$ and the velocity of each mode υ_{gi} play an essential role. For the net heat current, ∂_{Q12}, across the defect, between the two ends of the waveguide held at slightly different temperatures $T + \Delta T > T$. Let's obtain:

$$\partial Q_{12} = \frac{1}{\ell} \sum_i \frac{1}{(2\pi)^2} \times$$

$$\times \int dq \upsilon_{gi}(q) \hbar \omega_i(q) \sigma_i(\omega_i, q) \cdot \frac{\partial n(T, \omega_i(q))}{\partial T}. \qquad (34)$$

In general, the thermal conductivity is ensured by the phononic contribution and the electronic one, more than the magnetic contribution in the case of ferromagnetic metals.

In this work, the electronic contribution is investigated; where the heat is carried by charge majority carriers which are the electrons provided by the two states 1 and 2.

The thermal conductivities are presented in Fig. 7 as a function of temperature and group velocity. The calculation curves show that the heat transport contributions increase to reach a maximum value. The explanation of what has just been formulated is that the electrons are more excited from the valence band towards the conduction band and each mode has an electrons number and special feature. So, the thermal effect reduced the performance of electronic systems by thermal runaway.
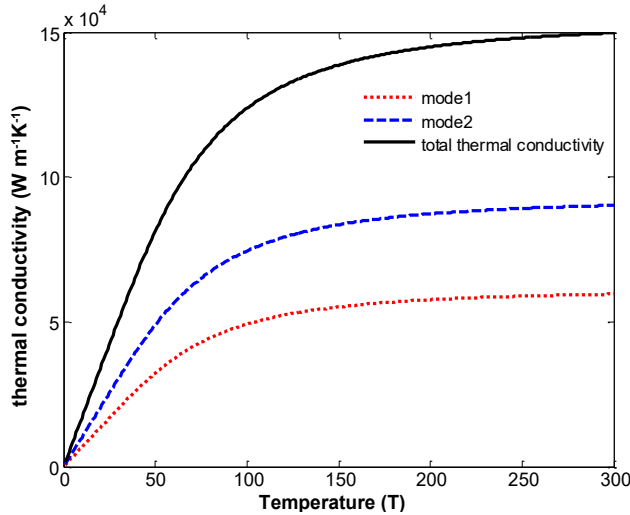
Fig. 7. The evolution of the thermal conductivity as a function of the temperature for each state (blue and red) and the total one (black color)

3.4. The densities of state. Electronic local density of state (LDOS) is one of the most important electronic properties that, informs about the behavior and electronic system nature. It also provides information about the nature of the chemical bonds between atoms. Indeed, it represents the energy per volume unit at 3D, energy per surface unit at 2D and energy per unit of length for a quantum wire as in our case; where it is obtained by using the square matrix M, resulted from the PMFT method and the Green functions [34–36] under the following operator form:

$$G(\omega+i\varepsilon,\varphi_x,Z)=\left[(\omega+i\varepsilon)I-M(\varphi_x,Z)\right]^{-1}. \qquad (35)$$

For a wave vector parallel to the direction of the defect chain, the local densities are given by the following equation:

$$\rho_\alpha^{(n,n')}(\omega,\varphi_x)=2\omega\sum_m L_{\alpha m}^n \cdot L_{\alpha m}^{*n'} \cdot \delta(\omega-\omega_m), \qquad (36)$$

where n and n' represent two different atomic sites, a Cartesian direction and $L_{\alpha m}^n$, $L_{\alpha m}^{n'}$ are the components a of the vector displacement of n and n' atoms, for the energy branch ω_m.

Finally, the density of states, which corresponds to the sum over φ_x, can then be given by the general form:

$$N(\omega)=\sum_{\varphi_x}\sum_{n\alpha}\rho_\alpha^{(n,n')}(\omega,\varphi_x)=$$

$$=-\frac{\omega}{\pi}\sum_{\varphi_x}\sum_{n\alpha}\lim_{\varepsilon\to 0}\left[\mathrm{Im}G_{\alpha\alpha}^{nn'}(\varphi_x,\omega+i\varepsilon)\right]. \qquad (37)$$

Based on the given expressions, let's represent in the various Fig. 8–11 the different local densities of state relating to the studied sites according to Table 2, which summarizes the ω value positions in different spectral peaks and theirs, height in arbitrary units.
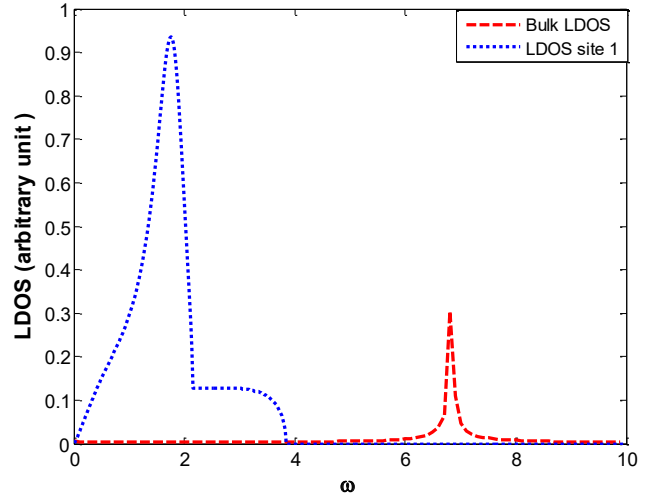
Fig. 8. The calculated LDOS for the atomic site 1
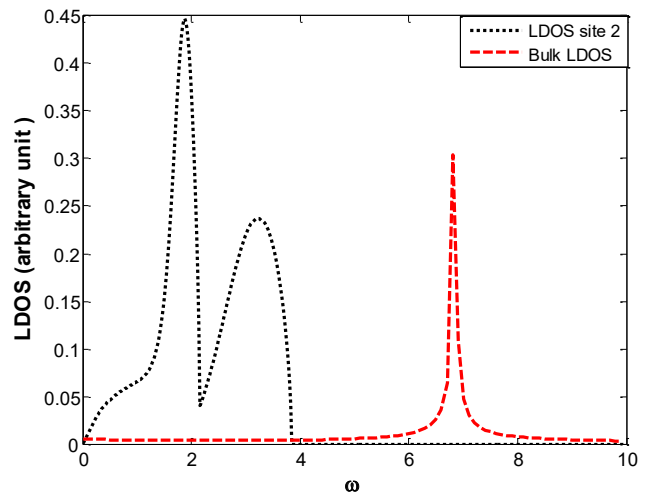
Fig. 9. The calculated LDOS for the atomic site 2
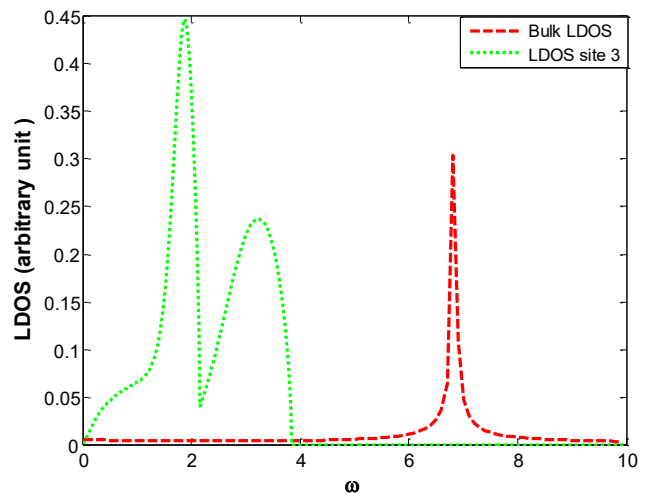
Fig. 10. The calculated LDOS for the atomic site 3
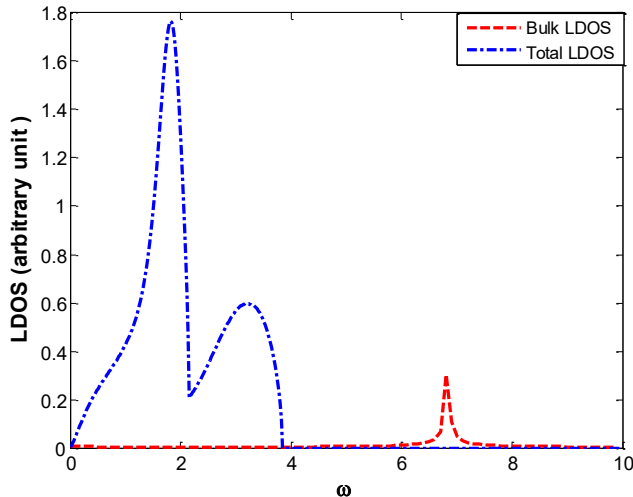
Fig. 11. The calculated LDOS for the bulk and LDOS of the perturbed zone

Table 2

The peaks position and their height in arbitrary units
in the LDOS spectra

Atomic sites	Width	Height
Bulk	$\omega=[6.4,\ 7.2]$	0.303
Total	$\omega=[0.78,\ 2.16]$ $\omega=[2.26,\ 3.76]$	1.767 0.596
Site (1)	$\omega=[0.44,\ 2.16]$	0.936
Site (2), (3)	$\omega=[1.32,\ 2.14]$ $\omega=[2.22,\ 3.82]$	0.446 0.237

In Fig. 8, the local density of state (LDOS) of site 1 of the doping atom has been represented; where, it is possible to notice that the curve presents a pick for $\omega=1.76$. It is the maximum of energetic amplitude corresponding to the contribution of the orbital s; its width informs us on the spectral distribution of the energy in the space of $\omega=[0.44,\ 2.16]$.

In Fig. 9 and 10, there are the LDOS of sites 2 and 3, where it is possible to notice that they are identical by symmetry to the system studied. Each one presents two peaks respectively for $\omega_1=1.88$ and $\omega_2=3.24$; the first is due to the contribution of the orbital s which is more energetic; the second is the contribution of the orbital p_x. The width of the density extends over $\omega=[1.32,\ 2.14]$ and $\omega=[2.22,\ 3.82]$ respectively; due to the spectral distributions of localized energies induced by the germanium impurity. The peak amplitude value of total local density of state shows that it is the sum of the partial densities of LDOS of the three irreducible sites of the system studied. Finally, in Fig. 11, the LDOS is represented for defect neighborhoods by comparing with that of bulk. It is possible to see that the energy amplitudes are larger and that the spectral distribution is more extensive while $\omega\in[0.76,\ 3.76]$, while for this of the bulk, there is one peak for $\omega=6.8$, and the spectral width is $\omega=[6.4,\ 7.2]$. Let's note that the bulk modes are located on the higher pulsation part.

3.5. Limitations and directions of research development. The study's findings on energy localization and electronic transport in germanium-doped silicon quantum wires offer significant practical applications across various fields.

Primarily, they enable the development of more efficient semiconductor devices with optimized electronic and thermal properties, leading to advancements in transistors, sensors, and quantum computing elements. Additionally, insights into defect-induced variations support the creation of non-destructive testing methods for higher quality control in material manufacturing. These advancements not only enhance current nano-electronic device technology but also pave the way for innovative applications in energy storage and conversion, contributing to sustainable energy solutions. Furthermore, the research methodologies and results serve as valuable educational tools for the next generation of scientists and engineers, fostering future innovations.

4. Conclusions

In this work, we focused our interests on the electronic properties of low-dimensional systems, which is an exciting and encouraging theme. With the Top-down and Bottom-up approach, it is now possible to develop low-dimensional systems from the quantum dot and the quantum wire to the systems 2D. These systems have interesting properties, notably the electronic and thermal conductivities, which deviate from the 3D system. We have examined from our work the electronic properties of a quantum silicon wire doped with a germanium atom. The appearance of this foreign atom breaks the translational symmetry in the direction which is perpendicular to it and makes the usual methods inappropriate and improper. There has been an introduction of a powerful mathematical method; the PMFT plays a crucial role in determining the different localization and scattering phenomena in a perturbed atomic chain by studying the electronic wave scattering by an impurity. Furthermore, the results reveal that the system conductance and the reflection and transmission coefficients appreciably vary with the atomic defect parameters. The variation of the conductance spectra may yield from the theoretical and experimental points of view, making use of useful information in the defect's neighborhood in specifics nano-structures. Moreover, we calculated the associated thermal conductivity, which is a measurable quantity and the electronic density of the states located in the neighborhood of the implanted defect. These states induced by the defect vanish on both sides of the impurity. Finally, it is essential to understand and comprehend how much atomistic modeling can be a powerful tool when developing new materials. If it has ever existed, the border between the basic and applied sciences is always more elegant. This narrow distinction is atomistic modeling out at once, exploring the development of their technological applications and underlying fundamental physical phenomenon.

Conflict of interest

The authors declare that they have no conflict of interest concerning this research, whether financial, personal,

authorship or otherwise, that could affect the study and its results presented in this paper.

Financing

Data availability

The paper has no associated data.

Use of artificial intelligence

The authors confirm that they did not use artificial intelligence technologies when creating this work.

References

1. Neuhaus, D.-H., Münzer, A. (2007). Industrial Silicon Wafer Solar Cells. *Advances in OptoElectronics, 2007*, 1–15. doi: https://doi.org/10.1155/2007/24521

2. Fuechsle, M., Miwa, J. A., Mahapatra, S., Ryu, H., Lee, S., Warschkow, O. et al. (2012). A single-atom transistor. *Nature Nanotechnology, 7 (4)*, 242–246. doi: https://doi.org/10.1038/nnano.2012.21

3. Ferrari, A. C., Bonaccorso, F., Fal'Ko, V., Novoselov, K. S., Roche, S., Bøggild, P. et al. (2015). Science and technology roadmap for graphene, related two-dimensional crystals, and hybrid systems. *Nanoscale, 7 (11)*, 4598–4810.

4. Waldrop, M. M. (2016). The chips are down for Moore's law. *Nature, 530 (7589)*, 144–147. doi: https://doi.org/10.1038/530144a

5. Luo, T., Chen, G. (2013). Nanoscale heat transfer – from computation to experiment. *Physical Chemistry Chemical Physics, 15 (10)*, 3389. doi: https://doi.org/10.1039/c2cp43771f

6. Luisier, M. (2014). Atomistic simulation of transport phenomena in nanoelectronic devices. *Chemical Society Reviews, 43 (13)*, 4357–4367. doi: https://doi.org/10.1039/c4cs00084f

7. Agraït, N., Yeyati, A. L., Van Ruitenbeek, J. M. (2003). Quantum properties of atomic-sized conductors. *Physics Reports, 377 (2-3)*, 81–279. doi: https://doi.org/10.1016/s0370-1573(02)00633-6

8. Sørensen, H. H. B., Hansen, P. C., Petersen, D. E., Skelboe, S., Stokbro, K. (2009). Efficient wave-function matching approach for quantum transport calculations. *Physical Review B, 79 (20)*. doi: https://doi.org/10.1103/physrevb.79.205322

9. Nitzan, A., Ratner, M. A. (2003). Electron Transport in Molecular Wire Junctions. *Science, 300 (5624)*, 1384–1389. doi: https://doi.org/10.1126/science.1081572

10. Ke, Y., Xia, K., Guo, H. (2008). Disorder Scattering in Magnetic Tunnel Junctions: Theory of Nonequilibrium Vertex Correction. *Physical Review Letters, 100 (16)*. doi: https://doi.org/10.1103/physrevlett.100.166805

11. Markussen, T., Rurali, R., Jauho, A.-P., Brandbyge, M. (2007). Scaling Theory Put into Practice: First-Principles Modeling of Transport in Doped Silicon Nanowires. *Physical Review Letters, 99 (7)*. doi: https://doi.org/10.1103/physrevlett.99.076803

12. Nozaki, D., Pastawski, H. M., Cuniberti, G. (2010). Controlling the conductance of molecular wires by defect engineering. *New Journal of Physics, 12 (6)*, 063004. doi: https://doi.org/10.1088/1367-2630/12/6/063004

13. Khater, A., Szczęśniak, D. (2011). A simple analytical model for electronic conductance in a one dimensional atomic chain across a defect. *Journal of Physics: Conference Series, 289*, 012013. doi: https://doi.org/10.1088/1742-6596/289/1/012013

14. Szczęśniak, D., Khater, A. (2012). Electronic conductance via atomic wires: a phase field matching theory approach. *The European Physical Journal B, 85 (6)*. doi: https://doi.org/10.1140/epjb/e2012-21055-x

15. Belayadi, A., Bourahla, B., Mekideche-Chafa, F. (2018). Localized electronic surface states in metallic structureS. *Surface Review and Letters, 25 (5)*, 1850101. doi: https://doi.org/10.1142/s0218625x18501019

16. Büttiker, M. (1986). Four-Terminal Phase-Coherent Conductance. *Physical Review Letters, 57 (14)*, 1761–1764. doi: https://doi.org/10.1103/physrevlett.57.1761

17. Landauer, R. (1957). Spatial Variation of Currents and Fields Due to Localized Scatterers in Metallic Conduction. *IBM Journal of Research and Development, 1 (3)*, 223–231. doi: https://doi.org/10.1147/rd.13.0223

18. Khomyakov, P. A., Brocks, G., Karpan, V., Zwierzycki, M., Kelly, P. J. (2005). Conductance calculations for quantum wires and interfaces: Mode matching and Green's functions. *Physical Review B, 72 (3)*. doi: https://doi.org/10.1103/physrevb.72.035450

19. Mardaani, M., Rabani, H., Esmaeili, A. (2011). An analytical study on electronic density of states and conductance of typical nanowires. *Solid State Communications, 151 (13)*, 928–932. doi: https://doi.org/10.1016/j.ssc.2011.04.010

20. Rabani, H., Mardaani, M. (2012). Exact analytical results on electronic transport of conjugated polymer junctions: Renormalization method. *Solid State Communications, 152 (3)*, 235–239. doi: https://doi.org/10.1016/j.ssc.2011.09.026

21. Wu, Y., Childs, P. (2010). Conductance of Graphene Nanoribbon Junctions and the Tight Binding Model. *Nanoscale Research Letters, 6 (1)*. doi: https://doi.org/10.1007/s11671-010-9791-y

22. Slater, J. C., Koster, G. F. (1954). Simplified LCAO Method for the Periodic Potential Problem. *Physical Review, 94 (6)*, 1498–1524. doi: https://doi.org/10.1103/physrev.94.1498

23. Harrison, W. A. (2004). *Elementary electronic structure (revised edition)*. World Scientific Publishing Company. doi: https://doi.org/10.1142/5432

24. Wills, J. M., Harrison, W. A. (1984). Further studies on interionic interactions in simple metals and transition metals. *Physical Review B, 29 (10)*, 5486–5490. doi: https://doi.org/10.1103/physrevb.29.5486

25. Landauer, R. (1957). Spatial Variation of Currents and Fields Due to Localized Scatterers in Metallic Conduction. *IBM Journal of Research and Development, 1 (3)*, 223–231. doi: https://doi.org/10.1147/rd.13.0223

26. Belayadi, A., Bourahla, B. (2018). A theoretical model to compute the localized electronic states at the surface of hexagonal structures with different coupling orbitals. *Surface Science, 675*, 1–14. doi: https://doi.org/10.1016/j.susc.2018.04.005

27. Bourahla, B., Nafa, O. (2016). Magnons Heat Transfer and Magnons Scattering in Magnetic Sandwich Lattices: Application to Fe/Gd(5)/Fe System. *SPIN, 6 (3)*, 1650007. doi: https://doi.org/10.1142/s2010324716500077

28. Bloch, F. (1929). Über die quantenmechanik der elektronen in kristallgittern. *Zeitschrift für physik, 52 (7-8)*, 555–600. doi: https://doi.org/10.1007/bf01339455

29. Feuchtwang, T. E. (1967). Dynamics of a Semi-Infinite Crystal Lattice in a Quasiharmonic Approximation. II. The Normal-Mode Analysis of a Semi-Infinite Lattice. *Physical Review, 155 (3)*, 731–744. doi: https://doi.org/10.1103/physrev.155.731

30. Szeftel, J., Khater, A. (1987). Calculation of surface phonons and resonances: the matching procedure revisited: I. *Journal of Physics C: Solid State Physics, 20 (29)*, 4725–4736. doi: https://doi.org/10.1088/0022-3719/20/29/010

31. Szczęśniak, D., Khater, A., Bąk, Z., Szczęśniak, R., Ghantous, M. A. (2012). Quantum conductance of silicon-doped carbon wire nanojunctions. *Nanoscale Research Letters, 7 (1)*. doi: https://doi.org/10.1186/1556-276x-7-616

32. Khater, A., Belhadi, M., Abou Ghantous, M. (2011). Phonons heat transport at an atomic well boundary in ultrathin solid films. *The European Physical Journal B, 80 (3)*, 363–369. doi: https://doi.org/10.1140/epjb/e2011-10892-8

33. Khater, A., Bourahla, B., Abou Ghantous, M., Tigrine, R., Chadli, R. (2011). Magnons coherent transmission and heat transport at ultrathin insulating ferromagnetic nanojunctions. *The European Physical Journal B, 82 (1)*, 53–61. doi: https://doi.org/10.1140/epjb/e2011-10935-2

34. Grimech, H., Khater, A. (1995). Calculation of the spectral densities of the surface alloy system (PtcCu1 – c1/Cu(100). *Surface Science, 323 (3)*, 198–206. doi: https://doi.org/10.1016/0039-6028(94)00630-x

35. Economou, E. N. (2006). *Green's functions in quantum physics. Vol. 7*. Springer Science & Business Media. doi: https://doi.org/10.1007/3-540-28841-4

36. Pastawski, H. M., Medina, E. (2001). *Tight Binding'methods in quantum transport through molecules and small devices: From the coherent to the decoherent description.* doi: https://doi.org/10.48550/arXiv.cond-mat/0103219

Aicha Zouaneb, Postgraduate Student, Department of Material Science, Laboratory of Energy Environment and Information System (LEEIS), African University Ahmed Draia, Adrar, Algeria, ORCID: https://orcid.org/0000-0002-0650-0044

✉*Elfahem Sakher, PhD, Lecturer, Department of Material Science, Laboratory of Energy Environment and Information System (LEEIS), African University Ahmed Draia, Adrar, Algeria; Associate Researcher, Environmental Research Center (C.R.E) sis at Alzone, Annaba, Algeria, e-mail: elf.sakher@univ-adrar.edu.dz, ORCID: https://orcid.org/0000-0002-0235-2873*

Tigrine Rachid, Professor, Department of Material Science, Laboratory of Energy Environment and Information System (LEEIS), African University Ahmed Draia, Adrar, Algeria, ORCID: https://orcid.org/0000-0003-4825-7625

Bendoura Abdallah, Postgraduate Student, Department of Material Science, Laboratory of Energy Environment and Information System (LEEIS), African University Ahmed Draia, Adrar, Algeria, ORCID: https://orcid.org/0000-0002-4718-4578

✉*Aissa Benselhoub, Associate Researcher, Environment, Modeling and Climate Change Division, Environmental Research Center (C.R.E), Annaba, Algeria, e-mail: benselhoub@yahoo.fr, ORCID: https://orcid.org/0000-0001-5891-2860*

✉*Corresponding author*